

Nuclear resonance small-angle scattering of x rays

Yu. V. Shvyd'ko

II. Institut für Experimentalphysik, Universität Hamburg, D-22761 Hamburg, Germany

A. I. Chumakov and A. Q. R. Baron

European Synchrotron Radiation Facility, BP 220, F-38043 Grenoble Cedex, France

E. Gerdau

II. Institut für Experimentalphysik, Universität Hamburg, D-22761 Hamburg, Germany

R. Rüffer

European Synchrotron Radiation Facility, BP 220, F-38043 Grenoble Cedex, France

A. Bernhard and J. Metge*

II. Institut für Experimentalphysik, Universität Hamburg, D-22761 Hamburg, Germany

(Received 1 July 1996)

A small-angle scattering technique is introduced for probing spatial variation of magnetization in solids with resolution down to $\sim 1 \mu\text{m}^{-1}$. The technique uses nuclear resonance scattering of synchrotron radiation. The sensitivity to spatial variation of magnetization due to domain walls and domain structure is demonstrated by small-angle scattering of 14.431 keV synchrotron radiation from ^{57}Fe nuclei in unmagnetized α - ^{57}Fe polycrystalline foils. [S0163-1829(96)08941-2]

Small-angle scattering of x rays (SAXS) and neutrons (SANS) have long been used to study inhomogeneities and disorder in matter on the linear scale from 1 nm to $1 \mu\text{m}$.^{1,2} Small-angle scattering of x rays is sensitive to the spatial variation of the electric charge density. Neutrons possess a magnetic moment, therefore small-angle neutron scattering is used as well to probe magnetic domain structure^{3,4} and critical magnetic fluctuations⁵ (for a review, see Ref. 6).

In the present paper we introduce a technique for probing magnetic spatial variation—nuclear resonance small-angle scattering of x rays (NSAXS). It became feasible only recently due to the appearance of synchrotron radiation sources of the third generation providing x-ray beams of high brilliance. The technique uses nuclear resonance scattering of synchrotron radiation (for reviews, see Refs. 7,8) and in particular its high sensitivity to the local magnetization, through the magnetic hyperfine fields, at each nucleus. If the magnetization in the sample is spatially homogeneous, then the response built up by all nuclear scatterers goes exactly into the primary beam direction—the so-called nuclear forward scattering (NFS) of synchrotron radiation.^{9,10} In this case the angular profile of the nuclear resonance response does not differ from the angular profile of the incident radiation. On the other hand, spatial variation of magnetization should cause scattering about the primary beam direction with angular spread inversely proportional to the characteristic length of the spatial variation. The angular-integrated intensity of nuclear resonance small-angle scattering should additionally characterize the value of the long-range spatial dispersion of magnetization. These different properties were studied in experiments presented in this paper.

The experiments were performed at the Nuclear Resonance Beamline¹¹ of the European Synchrotron Radiation

Facility. The storage ring was run with average electron current of 70 mA in 16-bunch mode producing undulator radiation pulses (~ 100 ps duration) every 176 ns. The 23 mm period undulator was tuned to provide 14.4 keV x rays in the fundamental. A double-crystal Si(1 1 1) premonochromator and the high-resolution monochromator^{12–14} in nested arrangement of Si(4 2 2) and Si(12 2 2) channel-cut crystals supplied radiation with 6.4 meV bandwidth at the x-ray energy of 14.413 keV (wavelength $\lambda = 0.8602 \text{ \AA}$) tuned to the nuclear resonance in ^{57}Fe , Fig. 1. The beam divergence in the horizontal (y, z) plane was $\approx 35 \mu\text{rad}$ and in the vertical (x, z) plane $\approx 15 \mu\text{rad}$. The beam size at the sample was reduced to $0.5 \times 0.5 \text{ mm}^2$ with slits before premonochromator.

The samples studied included unmagnetized polycrystalline foils of ferromagnetic metallic α - ^{57}Fe 2.5, 10, and $36 \mu\text{m}$ thick and the same foils in an 0.55 T external magnetic

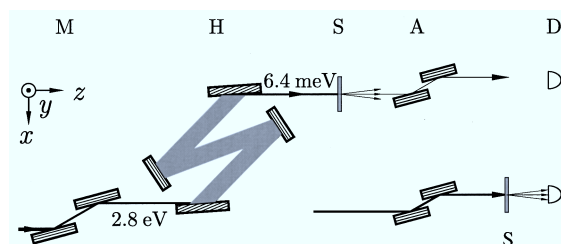


FIG. 1. Scheme of the experimental setup for angular-resolved nuclear resonant small-angle scattering: *M* is the Si(1 1 1) premonochromator; *H* is the Si(4 2 2) \times Si(12 2 2) high-resolution monochromator; *S* is the sample; *A* is the Si(1 1 1) analyzer; *D* is the detector. The inset shows the end part of the set-up modified for angular integrated scattering with the sample moved downstream of the Si(1 1 1) analyzer.

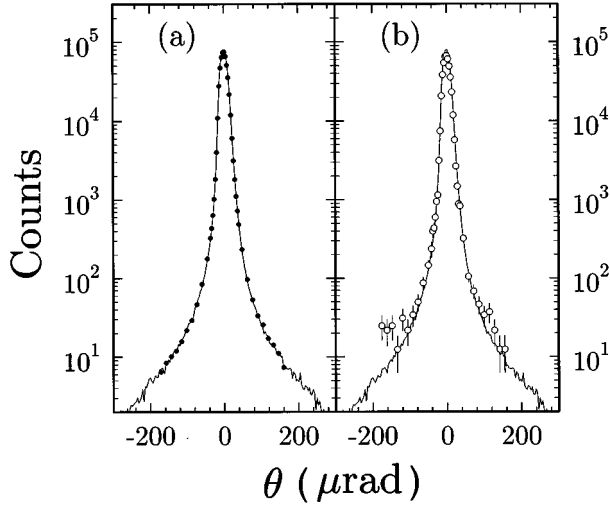


FIG. 2. Angular profiles of the (a) nonresonant and (b) nuclear resonant scattering from the 10 μm magnetized α - ^{57}Fe foil (\circ). The angular profiles of the incident radiation are presented in (a,b) by thin solid lines. The angular profiles of the nonresonant scattering from magnetized and unmagnetized foil are the same.

field directed parallel to the foil surface. All samples were enriched in ^{57}Fe to 95%.

The angular profile of the radiation emerging from a sample was measured by rocking the Si(1 1 1) analyzer installed downstream. It provided selectivity in the vertical scattering plane (acceptance angle $\approx 18 \mu\text{rad}$) and strong integration ($\approx \pm 10 \text{ mrad}$) in the horizontal plane. To perform additional measurements of angular-integrated nuclear resonance scattering about the primary beam direction a sample was shifted downstream of the Si(1 1 1) analyzer, see inset in Fig. 1.

The detector used was a reach-through avalanche photodiode¹⁵ with time resolution of 1 ns and background count rate less than 0.05 Hz. The long natural lifetime $\tau_0 = 141.1 \text{ ns}$ of the 14.413 keV excited state of ^{57}Fe nuclei allows easy discrimination of the delayed nuclear signal from the prompt signal of the electronic scattering. The nuclear response was measured by counting photons in the time window 15–160 ns after the excitation by a synchrotron radiation pulse. Electronic scattering (being the dominant process) was measured by counting photons without any time gating.

The angular profile of the incident radiation was measured by rocking the Si(1 1 1) channel-cut with no sample installed in the beam. It is shown by thin solid curves in Figs. 2(a), 2(b), and 3. Its full width at half maximum of $\delta = 20 \mu\text{rad}$ defines the resolution of the setup in the reciprocal space $\approx 2\pi\delta/\lambda = 1.5 \mu\text{m}^{-1}$. The angular profile of the radiation nonresonantly scattered from the 10 μm sample of the magnetized α - ^{57}Fe is shown in Fig. 2(a) by solid circles (for the unmagnetized sample it is the same). There is no difference in the angular profiles indicating homogeneous charge density in the foil. The angular profile of the resonant radiation emerging from the same foil given in Fig. 2(b) by open circles shows only a small difference to the angular profile of the incident radiation.

In contrast the resonant radiation emerging from unmag-

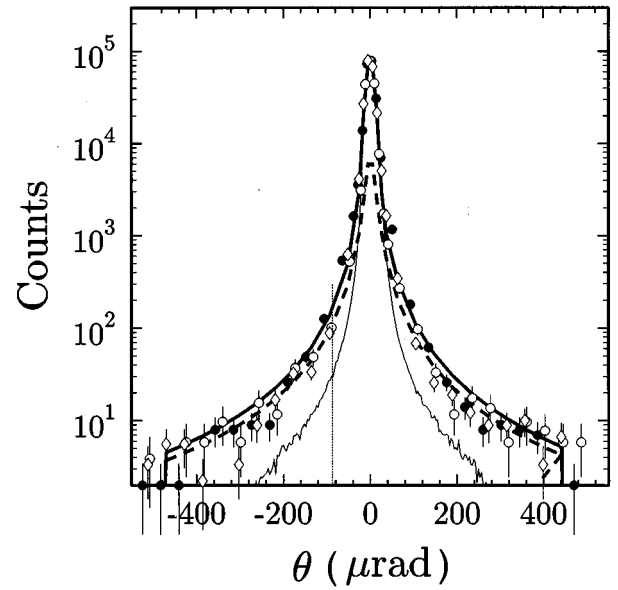


FIG. 3. Angular profiles of the nuclear resonant scattering from the 2.5 (\circ), 10 (\bullet), and 36 μm (\diamond) unmagnetized α - ^{57}Fe foils. Each angular point was measured for 30 s. The angular profile of the incident radiation is presented by the thin solid line. The bold solid line is a fit according to Eq. (1). The dashed line shows the angular profile of nuclear resonance small-angle scattering [Eq. (2)] in α - ^{57}Fe determined from the fit. The vertical line at $\theta = -87 \mu\text{rad}$ indicates the angular position of the Si (111) analyzer where the time spectra of small-angle scattering were measured; see Figs. 4(b) and 4(d).

netized samples of α - ^{57}Fe given by symbols in Fig. 3 shows considerable broadening compared to the incident radiation. We point out here the first observation: inhomogeneous magnetization, namely magnetic domain walls or (and) domains, which arises in α - ^{57}Fe after removal of the external magnetic field shows up immediately in the pure nuclear small-angle scattering.

The second observation is that the angular distributions of the nuclear scattering measured in samples of different thickness do not vary significantly from sample to sample. The angular profiles for the 2.5, 10, and 36 μm foils given in Fig. 3 by different symbols look very similar within the accuracy of the measurements. This suggests that despite the very large effective resonance thicknesses $L_{\text{eff}} = \sigma_{\text{res}} f_M N L$, which, e.g., in the case of the 36 μm α - ^{57}Fe foil amounts to $L_{\text{eff}} \approx 590$, the NSAXS might be considered in the first approximation as a single scattering process in contrast to NFS as a multiple one. Here σ_{res} is the resonance cross section, f_M is the Lamb-Mössbauer factor, N is the number of ^{57}Fe nuclei in the unit volume, and L is the foil thickness, respectively.

The angular dependences of nuclear scattering in Fig. 3 were fit (bold solid line) by using the equation

$$N(\theta) = I(\theta) + \int_{-\infty}^{+\infty} S(\theta - \theta') I(\theta') d\theta', \quad (1)$$

where θ is the rocking angle of the Si(1 1 1) analyzer in the (x, z) plane, $I(\theta)$ and $S(\theta)$ are the angular profiles of the

incident radiation and of nuclear resonance small-angle scattering, respectively. The vertically scattering analyzer crystal integrates over the scattering in the horizontal (y, z) plane. Thus, assuming the small-angle scattering from the sample is axially symmetric about the incident beam direction, one relates the measured response $S(\theta)$ to the real response function $R(Q)$ of nuclear resonance small-angle scattering by $S(Q_x) \propto \int dQ_y R(Q)$ where $Q = |Q_x \mathbf{x} + Q_y \mathbf{y}|$ is the value of the scattering vector and $Q_x = 2\pi\theta/\lambda$ is its x component. By integrating Eq. (1) one can find that $D = \int_{-\infty}^{+\infty} S(\theta) d\theta$ gives the relative value of the angular integrated NSAXS intensity normalized to the intensity of NFS. Analysis of the data shows that a good fit is achieved by choosing $S(\theta)$ as Lorentzian

$$S(\theta) = D \frac{\Delta\theta}{2\pi} \frac{1}{\theta^2 + (\Delta\theta/2)^2}, \quad (2)$$

with $\Delta\theta = 23 \pm 5 \mu\text{rad}$ and $D = 0.16 \pm 0.03$ (dashed line in Fig. 3). The response function is then given by

$$R(Q) \propto \frac{1}{[Q^2 + (q/2)^2]^{3/2}}, \quad (3)$$

where $q = 2\pi\Delta\theta/\lambda$.

Proceeding from the single scattering model one can argue that the response function of nuclear resonance small-angle scattering $R(Q)$ is the Fourier transform of the pair correlation (cf. Ref. 16) or characteristic (cf. Ref. 1) function of the spatial distribution of magnetization, while q^{-1} is the correlation length. The value $q^{-1} = 0.6 \mu\text{m}$ is in agreement with the domain-wall width in Fe, known to be in the range $0.3 \dots 1 \mu\text{m}$.^{17,18} The domain size, which in polycrystalline Fe is at least $10 \mu\text{m}$ ⁴ does not show up in the data, presumably due to the resolution limit in the reciprocal space of our setup. To establish the relationship between the correlation function and distribution of magnetization in domain walls a theory of nuclear resonance small-angle scattering is required.

It is noteworthy that the Lorentzian dependence of nuclear resonance small-angle scattering in Fe foils differs from the Gaussian dependence of small-angle neutron scattering observed in bulk samples of iron.^{3,4} Gaussian broadening, having \sqrt{L} dependence on the sample thickness, originates from the multiple character of small-angle neutron scattering. This multiple character of small-angle neutron scattering does not allow one to determine domain size directly from experimental data. Theoretical models are required.⁴ In contrast to the multiple small-angle neutron scattering the single nuclear resonance small-angle scattering provides undisturbed and direct information on the correlation function and correlation length of the spatial distribution of magnetization.

The third observation is derived from the comparison of the angular-integrated nuclear resonance small-angle scattering and nuclear forward scattering intensities. For this purpose the total number of counts N_{NFS} and N_{Σ} in the time window 15–165 ns were measured for each sample upstream and downstream of the Si(1 1 1) analyzer, respectively (see Fig. 1 and the inset). The analyzer was set at $\theta = 0$. N_{NFS} is proportional to the time-integrated intensity of nuclear forward

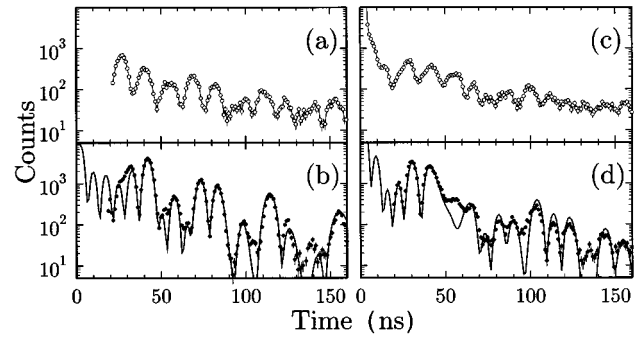


FIG. 4. Time spectra of the nuclear scattering in unmagnetized α - ^{57}Fe foils 2.5 μm (a,b) and 10 μm thick (c,d). The Si(1 1 1) analyzer was set at $\theta = 0$ (b, d) and at $\theta = -87 \mu\text{rad}$ (a, c). Solid lines in (b, d) are the calculated nuclear forward scattering time spectra in unmagnetized α - ^{57}Fe . The lines in (a, c) guide the eye.

ward scattering. The difference $N_{\Sigma} - N_{\text{NFS}}$ is proportional to the angular- and time-integrated intensity of NSAXS.¹⁹ The ratio

$$\mathcal{D} = \frac{N_{\Sigma} - N_{\text{NFS}}}{N_{\text{NFS}}} \quad (4)$$

appears to be the same $\mathcal{D} = 0.15 \pm 0.01$ (within the given error) for the three α - ^{57}Fe foils of different thickness. As one could expect, it is close to the value of the relative angular integrated intensity of NSAXS $D = 0.16 \pm 0.03$ obtained from the fit of the angular dependences in Fig. 3. As long as the intensity of nuclear forward scattering is a measure of spatial homogeneity and on the contrary the intensity of nuclear resonance small-angle scattering is a measure of spatial inhomogeneity, it is clear that \mathcal{D} (like D as well) can serve as a measure of the long-range spatial dispersion of magnetization in a given substance.

Figures 4(b) and 4(d) show time spectra of the nuclear resonance scattering with the Si(1 1 1) analyzer set at $\theta = 0$ (measured in 2.5 and 10 μm α - ^{57}Fe foils, respectively). They correspond to nearly pure nuclear forward scattering time spectra. Solid lines are the calculated nuclear forward scattering time spectra in unmagnetized α - ^{57}Fe . The spectra in Figs. 4(a) and 4(c) were measured in the same samples with the Si(1 1 1) analyzer set at $\theta = -87 \mu\text{rad}$ (vertical line in Fig. 3). These time spectra comprise 70% of NSAXS, i.e., the dominant part, and 30% of NFS. The time spectra in Figs. 4(a) and 4(c) are very different from that in Figs. 4(b) and 4(d). This is direct experimental proof that what we call nuclear resonance small-angle scattering is a scattering process different from nuclear forward scattering.

It should be noted that in the usual procedure of measuring the nuclear forward scattering time spectra no angular analyzer is used.¹⁰ Therefore in those cases where the relative amount of nuclear resonance small-angle scattering given by \mathcal{D} is large its contribution should be considered in processing the time spectra.

In summary, an experimental technique—nuclear resonance small-angle scattering of x rays—is introduced for probing spatial variation of magnetization in solids with resolution in reciprocal space down to $\sim 1 \mu\text{m}^{-1}$. It allows

one to measure the correlation function, the correlation length, and the dispersion of the long-range spatial variation of magnetization.

The technique can be used to probe magnetic domain structure. Due to the high brilliance of the contemporary synchrotron-radiation sources the studies of magnetic domains in special conditions, e.g., under high pressure, or other extreme conditions become accessible.

Along with magnetic hyperfine fields the nuclear resonance scattering is sensitive to electric-field gradients (EFG's) and the charge density at nuclei (via chemical shifts). Therefore nuclear resonance small-angle scattering might be also used to probe spatial variation of EFG and chemical bonding in solids.

The method could be especially attractive for studies of critical magnetic fluctuations. Along with the high resolution in reciprocal space to variation of magnetization (typical also for x-ray magnetic and neutron-diffraction techniques used so far for such studies^{20–22}) the proposed technique offers new possibilities: (1) Single crystals are not required as samples; any sample, including amorphous ones, can be studied. (2) It might be used to investigate relaxation times of critical magnetic fluctuations.

We would like to thank Dr. H.D. Rüter for helpful discussion. This work was funded by the Bundesministerium für Bildung, Wissenschaft, Forschung und Technologie under Contract No. 05 643 GUA 1 and by the European Synchrotron Radiation Facility.

*Present address: European Synchrotron Radiation Facility, BP 220, F-38043 Grenoble Cedex, France.

¹A. Guinier and G. Fournet, *Small-Angle Scattering of X-rays* (Wiley, New York, 1955).

²O. Glatter and R. May, in *International Tables for X-ray Crystallography*, edited by A.J.C. Wilson (Kluwer Academic, Dordrecht, 1992), Vol. C, pp. 81–112.

³D.J. Hughes, M.T. Burgy, R.B. Heller, and J.W. Wallace, *Phys. Rev.* **75**, 565 (1949).

⁴S.Sh. Shil'shtein, V.A. Somenkov, M. Kalanov, and N.O. Elyutin, *Sov. Phys. Solid State* **18**, 1886 (1976).

⁵D.J. Hughes and H. Palevsky, *Phys. Rev.* **92**, 202 (1953).

⁶M.F. Collins, *Magnetic Critical Scattering* (Oxford University Press, Oxford, 1989).

⁷E. Gerdau and U. van Bürck, in *Resonant Anomalous X-ray Scattering, Theory and Applications*, edited by G. Materlik, C.J. Sparks, and K. Fischer (North-Holland, Amsterdam, 1994), p. 589.

⁸G.V. Smirnov, *Hyperfine Interact.* **97/98**, 551 (1996).

⁹Yu. Kagan, A.M. Afanas'ev, and V.G. Kohn, *J. Phys. C* **12**, 615 (1979).

¹⁰J.B. Hastings, D.P. Siddons, U. van Bürck, R. Hollatz, and U. Bergmann, *Phys. Rev. Lett.* **66**, 770 (1991).

¹¹R. Rüffer and A.I. Chumakov, *Hyperfine Interact.* **97/98**, 589 (1996).

¹²T. Ishikawa, Y. Yoda, K. Izumi, C.K. Suzuki, X.W. Zhang, M. Ando, and S. Kikuta, *Rev. Sci. Instrum.* **63**, 1015 (1992).

¹³R. Rüffer (unpublished).

¹⁴T.M. Mooney, T.S. Toellner, W. Sturhahn, E.E. Alp, and S.D. Shastri, *Nucl. Instrum. Methods Phys. Res. Sect.* **347**, 348 (1994).

¹⁵A.Q.R. Baron, *Nucl. Instrum. Methods Phys. Res. Sect. A* **352**, 665 (1995).

¹⁶L. Van Hove, *Phys. Rev.* **95**, 249 (1954).

¹⁷M.K. Savchenko and V.I. Sinogubov, *Sov. Phys. JETP* **17**, 528 (1963).

¹⁸S. Müller-Pfeiffer, M. Schneider, and W. Zinn, *Phys. Rev. B* **49**, 15 746 (1994).

¹⁹Our measurement technique does not distinguish between NSAXS into angles smaller than 20 μ rad and NFS. Therefore the difference $N_{\Sigma} - N_{\text{NFS}}$ underestimates the real value of the angular- and time-integrated intensity of NSAXS.

²⁰T.R. Thurston, G. Helgesen, D. Gibbs, J.P. Hill, B.D. Gaulin, and G. Shirane, *Phys. Rev. Lett.* **70**, 3151 (1993).

²¹P.M. Gehring, K. Hirota, C.F. Majkrzak, and G. Shirane, *Phys. Rev. Lett.* **71**, 1087 (1993).

²²S. Langridge, W.G. Stirling, G.H. Lander, J. Rebizant, J.C. Spirlet, D. Gibbs, and O. Vogt, *Europhys. Lett.* **25**, 137 (1994).